ELSEVIER

Catalysis Today 78 (2003) 365–376

CATALYSIS TODAY

www.elsevier.com/locate/cattod

Nb_2O_5-supported WO_3: a comparative study with WO_3/Al_2O_3

C. Martín [a], G. Solana [a], P. Malet [b], V. Rives [a,*]

[a] *Departamento de Química Inorgánica, Universidad de Salamanca, 37008 Salamanca, Spain*

[b] *Departamento de Química Inorgánica e Instituto de Ciencia de Materiales, Centro Mixto Universidad de Sevilla, CSIC, Sevilla, Spain*

Abstract

WO_3/Nb_2O_5-supported samples prepared by impregnation are characterised by X-ray diffraction (XRD), Raman spectroscopy and X-ray absorption spectroscopy (XAS) at the W–L_3 absorption edge, as well as temperature programmed reduction (TPR) and FT-IR monitoring of pyridine adsorption. Results are compared with those obtained for WO_3/Al_2O_3 samples prepared in the same conditions, showing that niobia is able to disperse tungsta better than alumina does. Formation of a crystalline WO_3 needs larger tungsten contents on niobia than on alumina, since tungsten solution into niobia is easier than into alumina. Raman and XAS spectra recorded under ambient conditions suggest that similar WO_x species are formed on both supports at tungsten contents 0.5–1 theoretical monolayers; however, TPR results for the low tungsten loaded samples indicate that, when reduction starts (always at temperatures higher than 700 K under H_2/Ar flow) there is a larger concentration of tetrahedral [WO_4] species on alumina, than on niobia. Samples with low tungsten loading have been tested in isopropanol decomposition and ethylene oxidation, following both processes by FT-IR of adsorbed species up to 673 K. Results show that adsorption of ethylene on WO_3/Nb_2O_5 yields acetaldehyde and acetate at 473 K, while this adsorption is non-reactive either on the supports or on WO_3/Al_2O_3. Isopropanol adsorbs dissociatively on both supports, leading to acetone and propene formation on tungsta–niobia, but only propene on tungsta–alumina, probably due to the larger reducibility of the tungsten-containing phases.

Keywords: Surface acidity; Tungsta–niobia catalysts; Raman spectroscopy; X-ray absorption spectroscopy

1. Introduction

Tungsten oxide is well known as an effective catalyst in several acid-catalysed processes (isomerisation and olefin polymerisation, dehydration and esterification of alcohols, etc.) [1–5]. As vanadia and molybdena, its catalytic performance can be largely modified upon dispersing on oxide supports, where variables such as calcination temperature, nature of the supported phase and surface acidity–basicity, among others, are of paramount importance [6], as well as the nature of the support used. The precise nature of the surface metal oxide species depends on the nature of the oxide support, fraction of surface covered by the supported phase, the presence of impurities and doping agents, calcination temperature and the hydration degree of the support, as reported by several authors [7–14], who have studied by different experimental techniques (Raman spectroscopy, EXAFS, DRS, etc.) these solids in ambient (hydrated) conditions, as well as under the dehydrated conditions existing in situ during catalytic reactions. Alumina and silica are among the most widely used supports, but it has been also recognised that, in addition to providing larger dispersions, the support may also affect the properties of the catalyst itself.

We have previously reported on the effect of different supports on the properties of V_2O_5 and MoO_3 catalysts [15–25], as well as some studies on

* Corresponding author. Fax: +34-9-239-4574.
E-mail address: vrives@usal.es (V. Rives).

0920-5861/02/$ – see front matter
PII: S0920-5861(02)00301-2

supported WO_3 [26–30]. In the present work, we report on tungsta supported on niobia and alumina, our aim being to study the effect of the nature of the support, tungsta loading and calcination temperature on the physicochemical and surface properties of the catalysts. Characterisation has been carried out by applying several physicochemical techniques for the samples under ambient (hydrated) conditions (X-ray diffraction (XRD), Raman and EXAFS spectroscopies), as well as FT-IR monitoring of surface acidity by pyridine adsorption on previously dehydrated samples. Some of the samples have been tested in isopropanol decomposition and ethylene oxidation, by FT-IR spectroscopy monitoring.

Table 1
Description of the samples

Sample	W content (% w/w)	S_{BET} (m^2/g)	W loading (W/nm^2)
Al_2O_3	–	100	–
WA0.5	8.1	95	2.8
WA1	14.7	88	5.5
WA1/973	14.7	65	7.4
WA1/1273	14.7	28	17.2
WA2	24.8	75	10.8
Nb_2O_5	–	63	–
Nb_2O_5/973	–	11	–
WN0.5	5.1	57	2.9
WN1	9.5	51	6.1
WN1/973	9.5	12	25.9
WN2	17.0	44	12.7
WN3	23.0	37	20.4

2. Experimental

Samples were prepared by impregnation of supports (alumina C from Degussa and hydrated niobium oxide from Niobium Products Co. Inc., USA), with aqueous solutions of ammonium paratungstate (Fluka, Switzerland) using 10 ml of solution per gram of support. Both supports were calcined at 773 K, 12 h, previously to the impregnation step. The amount of tungsten salt dissolved was that necessary to obtain, after calcination, samples containing 0.5, 1, 2 and 3 theoretical monolayers of WO_3, assuming that a "molecule" of WO_3 covers a surface of 17×10^4 pm^2 [31] and the specific surface area of the calcined supports, as determined by the BET method (Al_2O_3 100 m^2/g; Nb_2O_5 63 m^2/g). The solvent was removed by evaporation in a water bath, and the solids thus obtained were dried at 373 K in air for 18 h, then manually ground in an agate mortar, and finally calcined in air for 3 h at 723 K. Samples are named as WS*X* (*X* standing for the number of theoretical monolayers of tungsta and S being A for alumina and N for niobia-supported samples). In order to analyse the effect of temperature on the nature of the active phase, WS1 samples were calcined in air up to 1273 K. These samples are named as WS1/T, T standing for the calcination temperature in K, as summarised in Table 1. Crystalline WO_3, used as a reference, was synthesised by calcination of ammonium paratungstate at 723 K.

XRD profiles were recorded under ambient conditions in a Siemens D-500 instrument, using graphite filtered Cu $K\alpha_1$ radiation ($\lambda = 154.05$ pm) interfaced to a DACO-MP data acquisition microprocessor equipped with Diffract-MP data acquisition software. *Nitrogen adsorption isotherms* at 77 K, for surface area and porosity determination, were carried out in a conventional high-vacuum Pyrex system (residual pressure $= 10^{-4}$ N/m^2), pressure changes being monitored with an MKS pressure transducer. The samples were previously degassed in situ at 423 K for 2 h. *Raman spectra* in the 200–1200 cm^{-1} range were recorded under ambient conditions on a computer controlled Jobin Yvon spectrometer, model U-1000, using the 514.5 nm line from a Spectra Physics model 165 Ar^+ laser as the exciting source. The spectra shift width was typically 5 cm^{-1}, and laser source powers at the sample were ca. 400 mW. *X-ray absorption* spectra data at the W–L_3 edge were collected at 77 K on wiggler station 9.2 at the Daresbury Synchrotron Radiation Source (UK), with an electron ring running at 2 GeV and 180–230 mA. Monochromatisation was obtained with a double silicon crystal monochromator working at the (2 2 0) reflection, which was detuned 50% to reduce higher harmonics. Measurements were carried out in transmission mode using optimised ion chambers as detectors. Sample powders, diluted with boron nitride when necessary, were ground, homogenised, and pressed into self-supported wafers, with edge jumps $\leq$1.0 just above the W–L_3 absorption edge (10 202 eV). At least three scans were recorded and averaged to obtain the experimental spectra. The EXAFS function $\chi(k)$ was obtained from the experimental X-ray absorption spectroscopy

(XAS) spectrum by conventional procedures [32]. Experimental backscattering amplitude and phase shift functions for W–O absorber–backscatterer pairs were extracted from the spectrum of $Al_2(WO_4)_3$, a compound where W(VI) cations are surrounded [33] by four oxygen atoms at 1.78 ± 0.03 Å (forward Fourier transform: k^3-weighted, $\Delta k = 2.4$–$15.5\,Å^{-1}$; inverse Fourier transform: $\Delta R = 0.6$–$2.2\,Å^{-1}$). EXAFS data analysis and handling were performed by using the program package XDAP [34]. *Temperature programmed reduction* (TPR) analysis was carried out on the samples, without any pretreatment, in a Micromeritics TPR/TPD 2900 instrument, at a heating rate of 10 K/min, using 60 ml/min of a H_2/Ar mixture as reducing agent (5 vol.% from L'Air Liquide, Spain). Experimental conditions for TPR runs were chosen according to data reported elsewhere [35] in order to reach good resolution of the component peaks. *Adsorption of pyridine, ethylene* and *2-propanol* was monitored by FT-IR spectroscopy. Samples were submitted to a conditioning treatment in situ, consisting of outgassing at 673 K for 2 h (residual pressure = 10^{-3} N/m^2), previous to the adsorption studies. Spectra were obtained with a Perkin-Elmer 16 PC spectrometer, connected to an Ataio 386-SX computer, and using special cells with CaF_2 windows.

3. Results and discussion

The specific surface area values determined following the BET method (S_{BET}) are given in Table 1. A steady decrease in S_{BET} is observed as the W content or the calcination temperature are increased. The cumulative surface area values and those determined from the *t*-plots are coincident with the S_{BET} values, as expected for mesoporous samples. XRD diagrams for alumina-supported samples are shown in Fig. 1. The diagram for alumina is typical of an ill-crystallised γ-alumina (JCPDS file 10-424). Only support lines

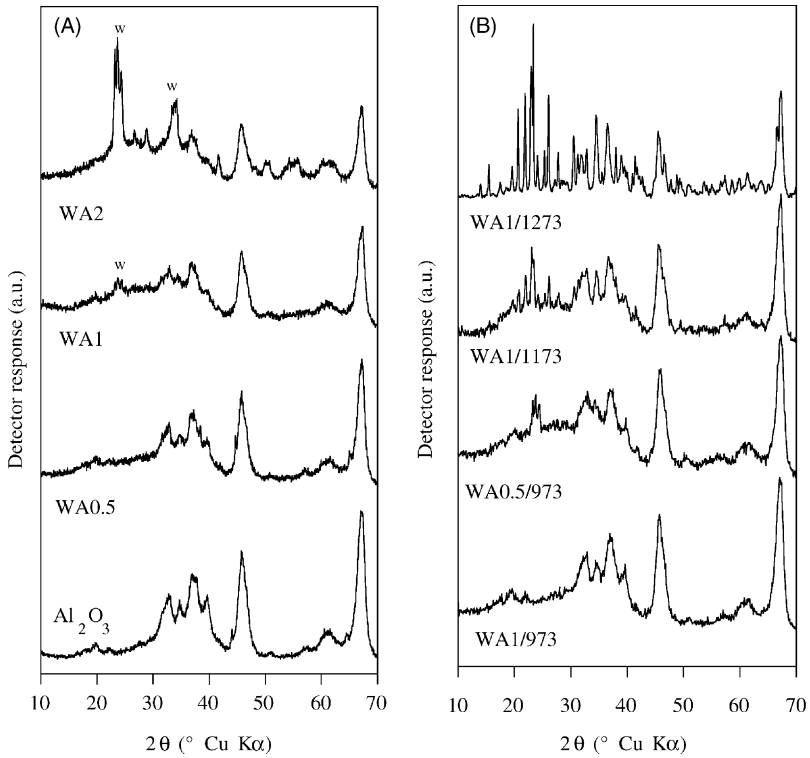

Fig. 1. XRD patterns of (A) alumina support and (B) selected WO_3/Al_2O_3 samples. Diffraction lines characteristic of crystalline WO_3 particles are denoted by w.

are recorded for sample WA0.5. Meanwhile, samples WA1 and WA2 show reflection lines characteristic of orthorhombic WO_3 at $2\theta = 24$–27° (JCPDS file 20-1324), thus showing that the experimental monolayer has been exceeded for tungsten loadings equal or higher than 5.5W/nm^2 (14.7% w/w). This result is in agreement with previous reports for hydrated samples [9,36], that found the experimental monolayer over alumina at 4.0–4.8W/nm^2. XRD pattern for sample WA1/973 is similar to that recorded for WA1, although lines ascribed to orthorhombic WO_3 slightly increase their intensity due to the decreased surface area. When calcination temperature is increased up to 1173 K, sample WA1/1173, the support partially transforms to θ-alumina (JCPDS file 11-517); diffraction lines characteristic of WO_3 disappear, while additional diffraction lines that can be ascribed to $Al_2(WO_4)_3$ (JCPDS file 28-36) develop. This transformation is complete after calcining at 1273 K. A similar reaction between tungsta and the alumina support, although at higher temperatures, was previously reported [37,38] and ascribed [38] to the migration of alumina over WO_3 particles.

XRD pattern of Nb_2O_5 support is characteristic of the pseudohexagonal modification (JCPDS file 7-61). After calcining at 973 K a partial transformation to orthorhombic L–Nb_2O_5 (JCPDS file 27-1003) is detected. XRD patterns recorded for WN1 and WN2 samples (Fig. 2) do not show diffraction lines different to those ascribed to the support, thus showing that niobia is able to disperse up to 12.7W/nm^2. Only after increasing tungsten loading up to three theoretical monolayers (sample WN3, 20.4W/nm^2), low intensity diffraction lines at 384 and 265 pm indicate that a small amount of crystalline WO_3 is formed. Previous reports [7,9,10] on WO_3/Nb_2O_5 samples prepared by incipient wetness and calcined at 773 K state that crystalline WO_3 is detected over the niobia support at tungsten contents higher than 3W/nm^2, a value slightly lower than that found, 4.0–4.8W/nm^2 [9,36], for WO_3/Al_2O_3 samples prepared by the same procedure. In our case, samples were prepared by immersion

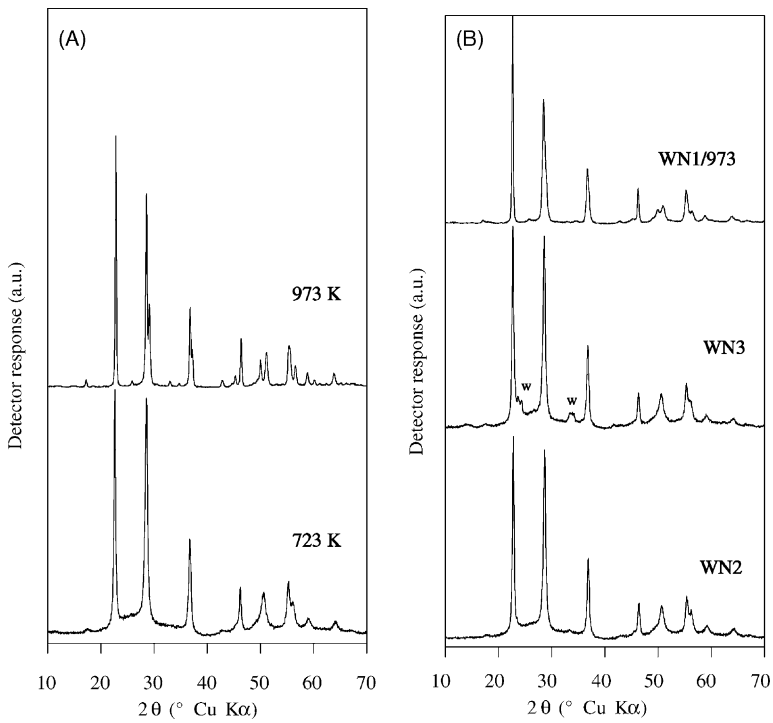

Fig. 2. XRD patterns of (A) niobia support and (B) selected WO_3/Nb_2O_5 samples. Diffraction lines characteristic of crystalline WO_3 are denoted by w.

of the support in the ammonium paratungstate solution and crystalline WO_3 was already detected, in agreement with previous reports, at 5.5W/nm^2 over the alumina support (sample WA1). However, XRD results show that niobia is able to disperse much higher tungsten loadings than previously reported. This result can be due to the incorporation of tungsten cations into the niobia support forming a solid solution under our preparation conditions. It is worth noting that after calcining at 973 K, and in spite of the decrease of the specific surface area, the XRD pattern recorded for WN1/973 does not show lines that could be ascribed neither to WO_3 nor to any other crystalline tungsten-containing compound. Diffraction lines ascribed to the support are slightly broadened after this thermal treatment, thus suggesting that a transformation to the orthorhombic phase has started. However, this transformation is retarded when compared to that observed for the bare support calcined at the same temperature, thus showing that tungsten has stabilised the pseudohexagonal modification of Nb_2O_5.

Raman spectra of air-exposed samples showed WO_3 bands for all samples where this oxide was identified by XRD. Positions and ascription of the main bands recorded are summarised in Table 2. The only features observed for samples WN0.5, WN1 and WN2 are two broad bands at 700 and 229 cm^{-1}, already recorded for the bare support. An additional band close to 800 cm^{-1}, that can be ascribed to microcrystalline WO_3 particles, and a weak band at 980 cm^{-1} are observed for WN3. This result is in agreement with a previous report by Jehng et al. [10], who observed for WO_3/Nb_2O_5 under ambient conditions, and after subtracting the support spectrum, Raman bands at ca. 980 and 880 cm^{-1}, that shifted to 1018 and 956 cm^{-1} after dehydration [7,10]. The Raman spectrum recorded for WA0.5 also shows a low intensity band close to 980 cm^{-1}. Increasing tungsten loading, sample WA1, intensifies this band and develops two new bands at 703 and 801 cm^{-1} that are the most intense in sample WA2, and can be ascribed to WO_3 particles. A band at 951–975 cm^{-1} was previously reported [12] as the most prominent feature of the Raman spectrum recorded under ambient conditions for WO_3/Al_2O_3 up to monolayer coverages. This band, ascribed to terminal ν(W=O) of hydrated surface species, shifted to 1004–1017 cm^{-1} after dehydrating the samples [7,13]. Thus, the band that we record close to 980 cm^{-1} may be ascribed to terminal ν(W=O) of well dispersed hydrated surface species [9]. Its position at high wave numbers suggests tetrahedral [WO_4] units, as ν(W=O) for these species was reported [39] in the range 913–1060 cm^{-1}, although it is very close to the highest limit accepted [39] for octahedral [WO_6] units (740–980 cm^{-1}). It was ascribed to octahedral surface species by Thomas and coworkers [40,41], while other authors [39,42,43] ascribed the band to tetrahedral [WO_4] units. More recently, Wachs and coworkers [9,10,12] proposed that under ambient conditions a thin water layer that dissolves tungsten species is present on the surface of the supports. An equilibrium is established in this

Table 2
Summary of Raman spectroscopy results

Sample	Bands (cm^{-1})	Ascription
WN0.5, WN1, WN2	229, 700	Support
WN3	229, 700	Support
	980	Terminal ν(W=O) of surface tungsten oxide
	800	ν(W=O) microcrystalline WO_3 particles
WA0.5	984	Terminal ν(W=O) of surface tungsten oxide
WA1	984	Terminal ν(W=O) of surface tungsten oxide
	801	ν(W=O) microcrystalline WO_3 particles
	703	Bending (W=O) microcrystalline WO_3 particles
WA2	984	Terminal ν(W=O) of surface tungsten oxide
	802	ν(W=O) microcrystalline WO_3 particles
	712	Bending (W=O) microcrystalline WO_3 particles
	268	δ(W–O–W)

aqueous solution, its pH value determining the polytungstate species formed. This pH value is defined by the pzc of the oxide support as well as by the loading of the supported phase. Thus, the presence of isolated WO_4^{2-} and paratungstate, $HW_6O_{21}^{5-}$, was proposed for WO_3/Al_2O_3 samples at submonolayer coverages [12], metatungstate [12] and $W_{12}O_{42}^{12-}$ [9] were proposed for monolayer WO_3/Al_2O_3 while $W_{12}O_{40}^{8-}$ was proposed [10] on hydrated WO_3/Nb_2O_5. These polytungstate species yield their most intense Raman bands close to 980 cm^{-1}, as well as weaker features at lower wavenumbers.

W–L_3 EXAFS spectra of polyoxotungstates have been reported [44]. Actually, we previously found [28] the formation of Keggin units in WO_3/SiO_2 samples prepared by impregnation of silica with aqueous solutions of ammonium metatungstate, and the presence of this compound was clearly shown by W–L_3 EXAFS spectroscopy. k^3-Fourier transforms of EXAFS data for polyoxotungstates [28,44], as well as those reported for other polyoxometallates [44,45], show intense signals close to 3.1 Å without phase shift correction, ascribed to M···M distances between edge-sharing [MO_6] octahedra. These signals appear at a distance significantly shorter than that found in the WO_3 structure, ∼3.5 Å without phase shift correction [28], where [WO_6] octahedra share vertex. Thus, W–L_3 EXAFS data, when measured under hydrated conditions, should be able to provide evidence of the presence of polytungstate species over the surface of the supports. Experimental EXAFS oscillations for air exposed sample WA1, and their associated k^3-weighted Fourier transforms (FT), are included in Fig. 3. EXAFS data for samples WA0.5 and WA1 under ambient conditions are nearly identical, thus suggesting a similar local surrounding of tungsten in both samples. Fig. 3 also includes EXAFS data obtained for orthorhombic WO_3, as well as those recorded for sample WA1/1273, where XRD data clearly indicated the presence of crystalline $Al_2(WO_4)_3$. FT of EXAFS data for bulk WO_3 shows two distinct maxima at 1.3 and 3.5 Å, without phase-shift correction. The first maximum is associated [28] to [WO_6] distorted octahedral units, with short (ca. 1.8–1.9 Å) and long (2.0–2.1 Å) W–O distances, while the 3.5 Å maximum arises [28] from single and multiple scattering effects in W–O–W bridges between vertex-sharing octahedra (W···W distances in the range 3.7–3.9 Å). Meanwhile, only the maximum close to 1.3 Å appears in the FT of EXAFS data for WA0.5, WA1 and WA1/1273, thus suggesting that W–O–W bridges that could be ascribed either to the presence of WO_3-like

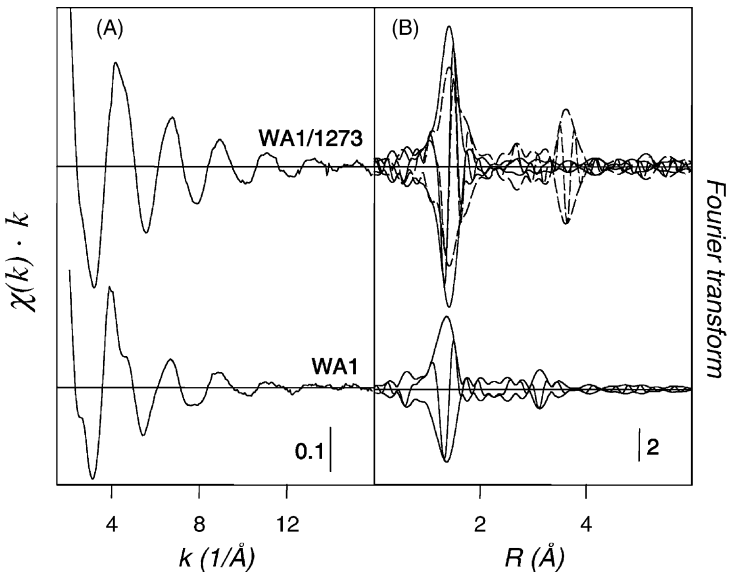

Fig. 3. WO_3/Al_2O_3 samples: (A) experimental EXAFS oscillations; (B) k^3-weighted Fourier transforms. Data for orthorhombic WO_3 are included for comparison (dashed lines).

Table 3
Best fit parameters for W–L_3 EXAFS spectra of WA and WN samples[a]

Sample	Atom	N	$\Delta\sigma^2$ (Å^2)	R (Å)	ΔE^0 (eV)
WA0.5	O	3.7	0.0030	1.78	3.2
	O	1.1	0.0070	2.00	7.1
WA1	O	3.6	0.0030	1.78	3.6
	O	1.1	0.0050	1.99	7.1
WN1	O	3.7	0.0025	1.78	5.6
	O	1.2	0.0043	1.98	7.6
WN1/973	O	4.4	0.0056	1.81	4.9
	O	1.8	0.0077	2.06	−7.2
WN2	O	3.7	0.0033	1.79	3.5
	O	1.8	0.0077	2.06	−1.5

[a] Estimated errors in coordination numbers (N) and shell radii (R) are ±15% and ±0.02 Å, respectively.

phases or to a polytungstate species are nearly absent in these samples. Actually, W···W distances shorter than 4 Å are not found in the structure [33] of $Al_2(WO_4)_3$, the main compound detected by XRD in sample WA1/1273. Fit results, within a single scattering approach, for WO_3/Al_2O_3 samples calcined at 723 K, are summarised in Table 3. W–O distances at the first coordination shell of tungsten are close to 1.8 and 2.0 Å, with an average coordination number 4.7, in close agreement with those reported by us [29] for air exposed WO_3/TiO_2 samples and suggesting a similar structure of the supported phase in both systems. Hilbrig et al. [46] reported W–O shell radii of 1.76 and 1.91 Å for an air exposed WO_3/TiO_2 sample containing 4.7W/nm^2, and found that the spectrum of this sample was identical to that recorded for an hydrated sample containing 1.6W/nm^2. They ascribed the shortest W–O distance to terminal W–O bonds and the longest W–O distance to W–O–Ti and W–O–W bridges, the latter yielding an additional well defined maximum close to 3.5 Å in the uncorrected FT. Meanwhile, Horsley et al. [39], reported XANES data at the W–L_1 absorption edge for alumina-supported samples. They found that only tetrahedral species [WO_4] were present at the dehydrated support surface for tungsten contents up to 1.4W/nm^2, and a significant fraction of the sites changed their coordination to octahedral [WO_6] after exposing these samples to air at room temperature. When coverage approached the monolayer, changes in the XANES spectra associated with the removal of the water molecules were much less evident, and distorted [WO_4] and [WO_6] units were present at the support surface. Our results, with an average of 4.7 oxygen atoms at the first coordination shell of tungsten, are consistent with the presence of [WO_4]/[WO_6] units, in agreement with the previous model, while the absence of a well defined maximum at 3.0–3.5 Å indicate a low polymerisation degree of [WO_x] units at the alumina surface.

Fig. 4 includes experimental EXAFS data for samples WN1, WN2 and WN1/973. Contribution of the nearest neighbours to the experimental oscillations were isolated (forward Fourier transform: k^3-weighted, Δk = 2.4–12.8 Å^{-1}; inverse Fourier transform ΔR = 0.3–2.3 Å). Best fit results to the first coordination shell are summarised in Table 3, showing that coordination parameters of tungsten cations for WN1 are similar to those obtained for samples WO_3/Al_2O_3 calcined at 723 K. Increasing either the WO_3 loading over niobia, sample WN2, or the calcination temperature, sample WN1/973, increased the number of oxygen atoms at the first coordination shell, mainly at the longest W–O distance, thus suggesting the formation of W–O–X bridges (X = W or Nb). As shown in Fig. 4A, these bridges raised intense signals at 3–3.7 Å for the sample calcined at 973 K. This result suggests that, at this temperature, tungsten is incorporated into the niobia support since, as reported above, only Nb_2O_5 is detected by XRD in this sample.

TPR profiles obtained for niobia and niobia-supported samples are shown in Fig. 5. Nb_2O_5 yields an intense maximum at 1100 K in all samples under study. Integrated hydrogen uptake for this maximum accounts for the reduction of ca. 50% of Nb(V) cations to Nb(IV). Tungsten-containing species are reduced in at least two steps that increases their intensity as the tungsten content does, an ill-defined maximum of low intensity close to 825 K and a well defined maximum at 990–1000 K. An additional maximum at high temperature, 1170 K, is recorded for WN samples calcined at 723 K. However, and although it is absent in the profile obtained for the bare support, its ascription to tungsten-containing species is not clear, since it has an intensity independent of tungsten loading. The behaviour observed for WN samples (for which hydrogen consumption amounts ca. 40–50% of the amount calculated for complete W(VI) → W(0) reduction),

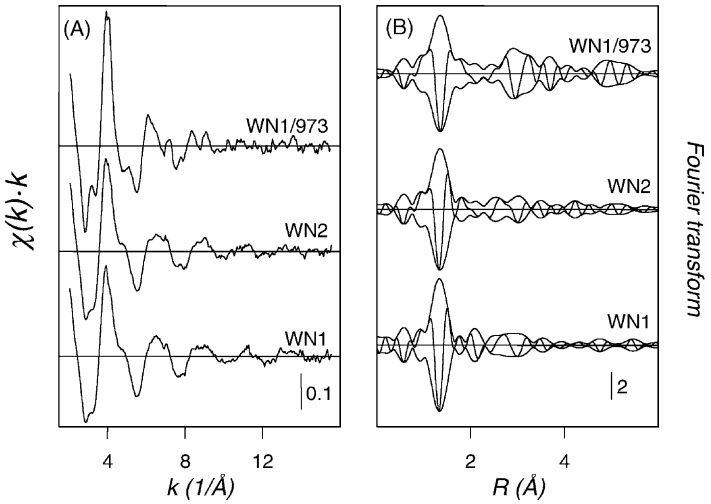

Fig. 4. WO_3/Nb_2O_5 samples: (A) experimental EXAFS oscillations; (B) k^3-weighted Fourier transforms.

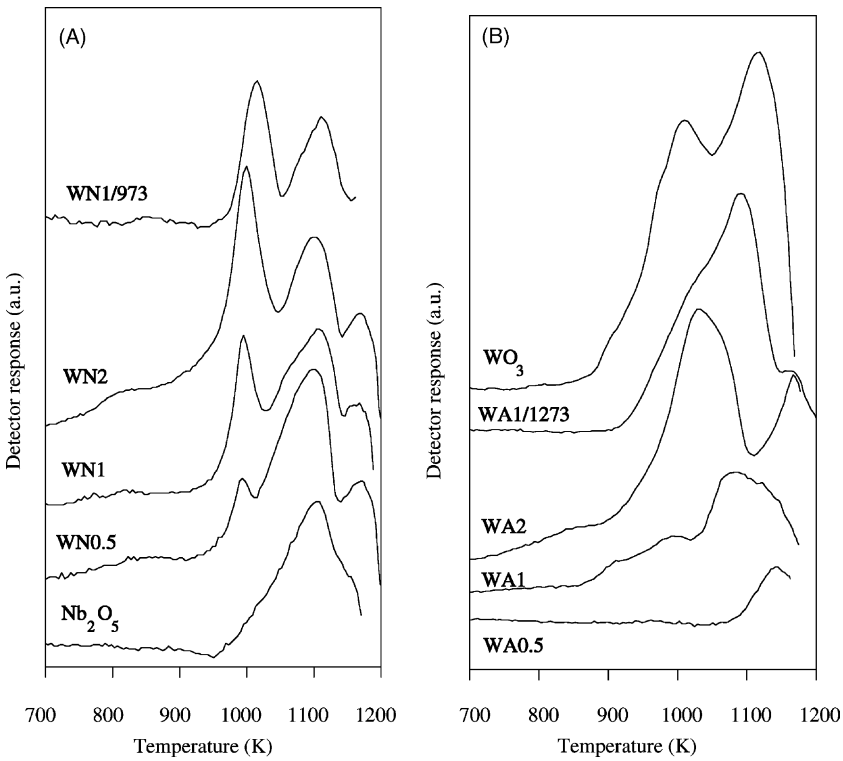

Fig. 5. TPR profiles recorded for (A) WO_3/Nb_2O_5 and (B) WO_3/Al_2O_3 samples.

Table 4
Position (cm^{-1}) and ascription of the main FT-IR bands recorded after adsorption of pyridine

Sample	Bpy[a]			Lpy[b]			
	8a	19a	19b	8a	8b	19a	19b
γ-Al_2O_3	–	–	–	1622, 1614, 1596	1579	1493	1449
WA0.5	1636	1490	1542	1614, 1594	1578	1490	1449
WA1	1638	1490	1540	1613, 1596 (sh)	1577	1490	1449
WA2	1637	1490	1538	1613	1577	1490	1449
WA1/1273	–	–	–	1614, 1612, 1596 (sh)	1577	1490	1448
Nb_2O_5	1635	1488	1540	1605	1574	1488	1444
WN0.5	1643	1487	1535	1608	1577	1487	1444
WN1	1635	1487	1535	1608	1576	1487	1444
WN2	1636	1489	1539	1609	1579	1489	1445
WN1/973	1635	1487	1535	1608	1576	1487	1444

[a] Protonated pyridine bonded to surface Brönsted acid sites.
[b] Pyridine coordinated to surface Lewis acid sites: sh denotes shoulder.

with reduction temperatures almost independent of the tungsten loading, contrasts with the strong dependence on tungsten content of the TPR profile recorded for WO_3/Al_2O_3 samples (Fig. 5). Thus, while WA0.5 only shows a reduction maximum at high temperature, 1150 K, increasing the tungsten loading develops reduction maxima at 920/980/1080 K for sample WA1 and 850/1030/1167 K for sample WA2. Integrated hydrogen uptakes for samples WA0.5, WA1 and WA2 account for 7, 32 and 43% of the amount necessary to complete the process $W(VI) \rightarrow W(0)$. Both data, reduction temperatures and hydrogen uptakes, clearly state that the reducibility of alumina-supported tungsten species decreases as tungsten loading decreases. EXAFS data above reported for air exposed WA0.5 and WA1 samples indicate the presence of rather similar WO_x species, with oxygen coordination number between 4 and 6, while TPR results demonstrate differences between the reducibility of these solids. However, it should be noticed that reduction during the TPR experiment starts always at temperatures higher than 700 K. Therefore, when reduction starts samples were dried in the carrier gas flow. As commented above, Horsley et al. [39] reported that the fraction of $[WO_6]$ species detected under ambient conditions for submonolayer alumina-supported samples disappears after drying 'in situ', yielding tetrahedral $[WO_4]$ species, while this effect is much less pronounced at a loading close to the monolayer, $[WO_4]$ and $[WO_6]$ species coexisting over the support surface even after drying 'in situ'. The maximum recorded at 1150 K for WA0.5 should be therefore ascribed to $[WO_4]$ species of low reducibility, while increasing the tungsten loading in WA1 develops new reduction maxima at lower temperatures that should be ascribed to octahedrally coordinated $[WO_6]$ species.

FT-IR spectra recorded after the adsorption of pyridine on WN samples, previously outgassed in situ as described in the experimental section, and after outgassing at room temperature show bands (Table 4) that can be ascribed to the stretching modes of coordinated and protonated pyridine, indicating the presence of surface Lewis and Brönsted acid sites, respectively. Both types of acid sites were already present for the niobia support. All bands remain after outgassing at increasing temperatures up to 573 K, thus indicating rather strong acidic sites. Only Lewis sites were detected for bare alumina (Table 4) while for WO_3/Al_2O_3 samples calcined at 723 K, FT-IR spectra of adsorbed pyridine also showed bands ascribed to Brönsted acid sites, that disappear for the sample calcined at 1273 K, a temperature at which $Al_2(WO_4)_3$ is formed. In both cases (when using supports alumina and niobia) the amount of Brönsted sites increased with the tungsten content. Such a change in the surface acidity of oxides when mixed with other oxides has been previously reported in the literature, and several models have been suggested to account for this change. Tanabe and Takeshita [47] ascribed this effect to the presence of charge-unbalanced, lo-

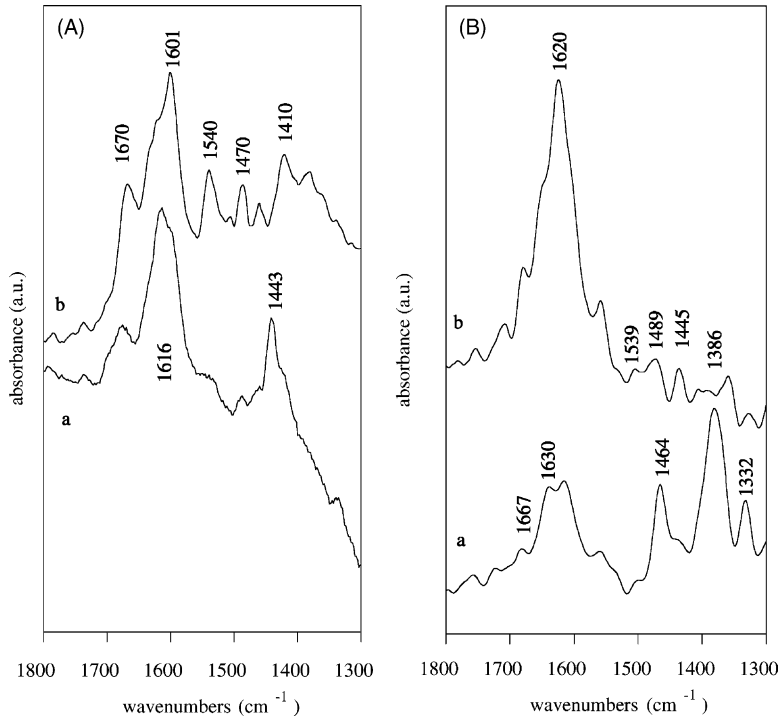

Fig. 6. FT-IR spectra of (A) ethylene adsorbed on sample WN1 at (a) 150 K and (b) 373 K, and (B) isopropanol adsorbed on sample WN1 at (a) room temperature and (b) 573 K.

calised M–O–X bonds (X being the new, in our case W, cation) formed in the mixed oxide. Kung [48] has suggested an unlocalised model. Both models are applied to diluted oxide mixtures, where cation substitution takes place. An alternative model has been proposed by Connell and Dumesic [49,50] for mixed oxides where such a cation substitution does not take place, but only incorporation of the "guest" onto the surface of the oxide support; these authors assume that the formal charge of the supported cation is balanced by surface coordination of lattice oxide anions, leading, in some cases, to coordinatively unsaturated cations able to behave as surface Lewis acid sites. The strength of these sites depends on the electronegativity of the guest metal cation.

Adsorption of ethylene on the supports and on WO_3/Al_2O_3 samples is non-reactive up to 673 K. Only weak interactions with the surface of the samples may be inferred from the shift of the ν(C=C) mode to lower wave numbers after adsorption of ethylene at 150 K (1625 cm^{-1} in the Raman spectrum of gaseous ethylene; 1620 and 1610 cm^{-1} after adsorption on Al_2O_3 and Nb_2O_5, respectively). This interaction has been ascribed [51] to σ-bonding between the π system of the olefin and empty orbitals of the support cation, that is favoured for transition metal cations with empty d orbitals. Adsorption of ethylene at 150 K on sample WN1 (Fig. 6) yields bands at 1616 cm^{-1}, ν(C=C), and 1443 cm^{-1}, $\delta_{as}(CH_2)$, also ascribed to non-reactive adsorption. After increasing the temperature to 473 K new bands are recorded at 1670, 1638 (shoulder), 1616 (shoulder), 1601, 1540, 1470 and 1410 cm^{-1}, that remain up to 673 K. Bands close to 1540 and 1470 cm^{-1} are also recorded after adsorbing acetic acid over this sample, and can be ascribed to ν_{as}(COO) and ν_s(COO), respectively, of acetate species. The band at 1670 cm^{-1} is characteristic of ν(CO) of coordinated acetaldehyde, and the bands at 1638 and 1616 cm^{-1} correspond to decomposition products of acetaldehyde.

Adsorption of isopropanol at room temperature in the absence of oxygen on sample WA1 leads to

a FT-IR spectrum with bands at 1468, 1397, 1391, 1336, 1165 and 1138 cm^{-1}, which are characteristic of isopropoxide species, as a result of dissociative adsorption; an additional band at 1286 cm^{-1} is due to physisorbed molecular isopropanol. Another band at 1616 cm^{-1} corresponds to $\delta(H_2O)$ mode, because of water formation through reaction of isopropanol with surface basic hydroxyl groups. When the sample is heated at 473 K this band becomes broader, because of development of a new band at 1638 cm^{-1} due to ν(C=C) mode of molecularly adsorbed propene, formed via dehydration of the alcohol, through the π C–C bond to exposed coordinatively unsaturated metal cations.

Adsorption on sample WN1 (Fig. 6) gives rise also to bands originated by both modes of adsorption, as isopropoxide species (bands at 1465, 1386, 1369, 1332, 1165 and 1114 cm^{-1}) and non-dissociative (1260 cm^{-1}). Formation of propene (band at 1640 cm^{-1}) is also observed, as in the case of adsorption on alumina, on increasing the temperature, while new bands at 1710 and 1682 cm^{-1}, due to ν(C=O) mode of acetone, also develop.

The higher activity of sample WN1 than sample WA1 for the reactions studied (formation of acetaldehyde and acetate from ethylene, and of acetone from isopropanol) should be undoubtedly related to the easier reducibility of tungsten when supported on niobia than when supported on alumina.

4. Conclusions

Tungsten precursors react differently on niobia than on alumina. Such a difference can be due to the different surface concentration and reactivity of hydroxyl groups on the surface of alumina and niobia, or to migration of tungsten inside the niobia crystallites. No crystalline species are detected on niobia and for low tungsten loadings, neither dispersed species are observed by Raman spectroscopy; however, microcrystalline species are detected for loadings equivalent to 20.36W/nm^2. EXAFS suggests the presence of $[WO_4]/[WO_6]$ species for loadings equivalent to monolayer or submonolayer coverages. Crystalline WO_3 is already detected, however, on alumina for a loading equivalent to 5.5W/nm^2. The different nature of the WO_x species existing on both supports for low loadings is evidenced in the easier reducibility of the phases supported on niobia, which gives rise to a larger activity of these systems in oxidation of ethylene to acetaldehyde and acetate species, and of isopropanol to acetone.

Acknowledgements

Financial support from Junta de Castilla y León (grant 71/99) is greatly acknowledged. We thank Daresbury Laboratory (UK) for allocating beam time for XAS measurements (Grant 25/359).

References

[1] I. Wender, Catal. Rev. 26 (1984) 304.
[2] M.I. Zaki, N. Sheppard, J. Catal. 80 (1983) 114.
[3] B. Grybowska-Swierkosz, Mater. Chem. Phys. 17 (1987) 121.
[4] A. Ouqour, G. Coudurier, J.C. Vedrine, J. Chem. Soc., Faraday Trans. 89 (1993) 1591.
[5] J. Haber, J. Janas, M. Schiavello, J.D. Tilley, J. Catal. 82 (1993) 395.
[6] K. Van der Wiele, P.J. Van der Berg, in: C.H. Bamford, C.F.H. Tipper (Eds.), Comprehensive Chemical Kinetics: Complex Catalytic Processes, Elsevier, Amsterdam, 1978.
[7] D.S. Kim, M. Ostromecki, I.E. Wachs, J. Mol. Catal. A: Chem. 106 (1996) 93.
[8] D.S. Kim, M. Ostromecki, I.E. Wachs, S.D. Kohler, J.G. Ekerdt, Catal. Lett. 33 (1995) 209.
[9] I.E. Wachs, Catal. Today 27 (1996) 437.
[10] J.-M. Jehng, A.M. Turek, I.E. Wachs, Appl. Catal. A 83 (1992) 179.
[11] I.E. Wachs, J.-M. Jehng, G. Deo, B.M. Weckhuysen, V.V. Guliants, J.B. Benziger, Catal. Today 32 (1996) 47.
[12] M.M. Ostromecki, L.J. Burcham, I.E. Wachs, N. Ramani, J.G. Ekerdt, J. Mol. Catal. A 132 (1998) 43.
[13] M.M. Ostromecki, L.J. Burcham, I.E. Wachs, J. Mol. Catal. A 132 (1998) 59.
[14] M.A. Bañares, I.E. Wachs, J. Raman Spectrosc. 33 (2002) 359.
[15] C. Martín, I. Martín, V. Rives, J. Catal. 145 (1994) 239.
[16] C. Martín, I. Martín, V. Rives, J. Chem. Soc., Faraday Trans. 89 (1993) 4131.
[17] M. Del Arco, S.R.G. Carrazán, C. Martín, I. Martín, V. Rives, P. Malet, J. Mater. Chem. 3 (1993) 1313.
[18] C. Martín, I. Martín, V. Rives, P. Malet, J. Catal. 147 (1994) 465.
[19] C. Martín, I. Martín, V. Rives, B. Gryzbowska, I. Gressel, Spectrochim. Acta A 52 (1996) 733.
[20] C. Martín, I. Martín, V. Rives, P. Malet, J. Catal. 161 (1996) 87.
[21] C. Martín, D. Klissurski, J. Rocha, V. Rives, Phys. Chem. Chem. Phys. 2 (1999) 1543.

[22] C. Martín, I. Martín, V. Rives, J. Mol. Catal. 73 (1992) 51.
[23] C. Martín, M.J. Martín, V. Rives, Stud. Surf. Sci. Catal. 72 (1992) 415.
[24] M. Del Arco, M.J. Holgado, C. Martín, V. Rives, Langmuir 6 (1990) 801.
[25] M. Del Arco, M.J. Holgado, C. Martín, V. Rives, J. Catal. 99 (1986) 19.
[26] C. Martín, V. Rives, G. Solana, React. Kinet. Catal. Lett. 58 (1996) 243.
[27] C. Martín, P. Malet, V. Rives, G. Solana, J. Catal. 169 (1997) 516.
[28] C. Martín, P. Malet, G. Solana, V. Rives, J. Phys. Chem. B 102 (1998) 2759.
[29] P. Malet, C. Martín, G. Solana, V. Rives, Aspects of the Surface Chemistry of Oxidic Systems, Edizioni Librería Cortina, Torino, Italy, 1999, p. 39.
[30] S.R.G. Carrazán, C. Martín, G. Solana, V. Rives, Langmuir 17 (2001) 6968.
[31] D.C. Vermaine, P.C. van Berge, C. Pieter, J. Catal. 116 (1989) 309.
[32] D.E. Sayers, B.A. Bunker, in: D.C. Koningsberger, R. Prins (Eds.), X-ray Absorption: Principles of EXAFS, SEXAFS and XANES, Wiley, New York, 1988.
[33] J.J. de Boer, Acta Cryst. B 30 (1974) 1878.
[34] http://www.xsi.nl.
[35] P. Malet, A. Caballero, J. Chem. Soc., Faraday Trans. 1 84 (1988) 2369.
[36] S.S. Chan, I.E. Wachs, L.L. Murrell, N.C. Dispenziere Jr., J. Catal. 92 (1985) 1.
[37] S.S. Chan, I.E. Wachs, L.L. Murrell, N.C. Dispenziere Jr., Catalysis on the Energy Scene, Elsevier, London, 1984, p. 259.
[38] L.L. Murrell, R.L. Garten, Appl. Surf. Sci. 19 (1984) 218.
[39] J.A. Horsley, I.E. Wachs, J.M. Brown, G.H. Via, F.D. Hardcastle, J. Phys. Chem. 91 (1987) 4014.
[40] R. Thomas, M.C. Mittelmeijer-Hazeleger, F.P.J.M. Kerkhof, J.A. Moujlin, J. Medema, V.H.J. de Beer, in: H.F. Barry, P.C.H. Mitchell (Eds.), Proceedings of the Third International Conference on the Chemistry and Uses of Molybdenum, Climax Molybdenum Co., Ann Arbor, MI, 1979, p. 85.
[41] R. Thomas, J.A. Moujlin, J. Mol. Catal. 15 (1982) 157.
[42] L. Salvati, L.E. Makovsky, J.M. Stencel, F.R. Brow, D.M. Hercules, J. Phys. Chem. 85 (1981) 3700.
[43] S.S. Chan, I.E. Wachs, L.L. Murrell, L. Wang, W.K. Hall, J. Phys. Chem. 88 (1984) 5831.
[44] J. Evans, M. Pillinger, J.M. Rummey, J. Chem. Soc., Dalton Trans. (1996) 2951.
[45] T. Miyanaga, T. Fujikawa, N. Matsubayashi, T. Fukumoto, K. Yokoi, I. Watanabe, S. Ikeda, Bull. Chem. Soc. Jpn. 62 (1989) 1791.
[46] F. Hilbrig, H.E. Göbel, H. Knözinger, H. Schmelz, B. Lengeler, J. Phys. Chem. 95 (1991) 6973.
[47] K. Tanabe, T. Takeshita, Adv. Catal. 17 (1967) 315.
[48] H. Kung, J. Solid State Chem. 52 (1984) 191.
[49] G. Connell, J.A. Dumesic, J. Catal. 102 (1986) 103.
[50] G. Connell, J.A. Dumesic, J. Catal. 102 (1986) 216.
[51] G. Busca, V. Lorenzelli, G. Ramis, V. Sanchez-Escribano, Mater. Chem. Phys. 29 (1991) 175.